

# Photometric redshifts with Quasi Newton Algorithm (MLPQNA). Results in the PHAT1 contest.

S. Cavuoti<sup>1,2</sup>, M. Brescia<sup>2,1</sup>, G. Longo<sup>1,2,3</sup>, and A. Mercurio<sup>2</sup>

<sup>1</sup> Department of Physics, Federico II University, via Cinthia 6, I-80126 Napoli, Italy e-mail: cavuoti@na.infn.it

<sup>2</sup> INAF - Astronomical Observatory of Capodimonte, via Moiariello 16, I-80131 Napoli, Italy

<sup>3</sup> Visiting associate - Department of Astronomy, California Institute of Technology, CA 90125, USA

Received June 2012; accepted August 2012

## ABSTRACT

*Context.* Since the advent of modern multiband digital sky surveys, photometric redshifts (photo-z's) have become relevant if not crucial to many fields of observational cosmology, from the characterization of cosmic structures, to weak and strong lensing.

*Aims.* We describe an application to an astrophysical context, namely the evaluation of photometric redshifts, of MLPQNA, a machine learning method based on Quasi Newton Algorithm.

*Methods.* Theoretical methods for photo-z's evaluation are based on the interpolation of a priori knowledge (spectroscopic redshifts or SED templates) and represent an ideal comparison ground for neural networks based methods. The MultiLayer Perceptron with Quasi Newton learning rule (MLPQNA) described here is a computing effective implementation of Neural Networks for the first time exploited to solve regression problems in the astrophysical context and is offered to the community through the DAMEWARE (Data Mining & Exploration Web Application REsource) infrastructure.

*Results.* The PHAT contest (Hildebrandt et al. 2010) provides a standard dataset to test old and new methods for photometric redshift evaluation and with a set of statistical indicators which allow a straightforward comparison among different methods. The MLPQNA model has been applied on the whole PHAT1 dataset of 1984 objects after an optimization of the model performed by using as training set the 515 available spectroscopic redshifts. When applied to the PHAT1 dataset, MLPQNA obtains the best bias accuracy (0.0006) and very competitive accuracies in terms of scatter (0.056) and outlier percentage (16.3%), scoring as the second most effective empirical method among those which have so far participated to the contest. MLPQNA shows better generalization capabilities than most other empirical methods especially in presence of underpopulated regions of the Knowledge Base.

**Key words.** techniques: photometric - galaxies: distances and redshifts- galaxies: photometry - cosmology: observations - methods: data analysis

## 1. Introduction

Estimating redshifts of celestial objects is one of the most pressing technological issues in the observational astronomy and, since the advent of modern multiband digital sky surveys, photometric redshifts (photo-z's) have become fundamental when it is necessary to know the distances of million of objects over large cosmological volumes. Photo-z's provide redshift estimates for objects fainter than the spectroscopic limit, and result much more efficient in terms of the number of objects per telescope time with respect to spectroscopic ones (spec-z). For these reasons, after the advent of modern panchromatic digital surveys, photo-z's have become crucial. For instance, they are essential in constraining dark matter and dark energy studies by means of weak gravitational lensing, for the identification of galaxy clusters and groups (e.g. Capozzi et al. 2009), for type Ia supernovae, and to study the mass function of galaxy clusters (Albrecht et al., 2006; Peacock et al., 2006; Keiichi et al., 2012). The need for fast and reliable methods for photo-z evaluation will become even greater in the near future for the exploitation of ongoing and planned surveys. In fact, future large field public imaging projects, like KiDS (Kilo-Degree Survey<sup>1</sup>), DES (Dark Energy Survey<sup>2</sup>), LSST (Large Synoptic Survey Telescope<sup>3</sup>), and Euclid

(Euclid Red Book 2011), require extremely accurate photo-z's to obtain accurate measurements that does not compromise the surveys scientific goals. This explains the very rapid growth in the number of methods which can be more or less effectively used to derive photo-z's estimates, and the efforts made to better understand and characterize their biases and systematics. The possibility to achieve a very low level of residual systematics (Huterer et al., 2006; D'Abrusco et al., 2007), is in fact strongly influenced by many factors: the observing strategy, the accuracy of the photometric calibration, the different point-spread-function in different bands, the adopted de-reddening procedures, etc. The evaluation of photo-z's is made possible by the existence of a rather complex correlation existing between the fluxes as measured in broad band photometry, the morphological types of the galaxies and their distance. The search for such correlation (a non-linear mapping between the photometric parameter space and the redshift values) is particularly suited for data mining methods. Existing methods can be broadly divided into two large groups: theoretical and empirical methods. Theoretical methods use templates, like libraries of either observed galaxy spectra or model Spectral Energy Distributions (SEDs). These templates can be shifted to any redshift and then convolved with the transmission curves of the filters used in the photometric survey to create the template set for the redshift estimators (e.g. Koo 1999, Massarotti et al. 2001a, Massarotti et al. 2001b, Csabai et al. 2003). However, for datasets in which accurate and multiband

<sup>1</sup> <http://www.astro-wise.org/projects/KIDS/>

<sup>2</sup> <http://www.darkenergysurvey.org/>

<sup>3</sup> <http://www.lsst.org/lst/>

photometry for a large number of objects are complemented by spectroscopic redshifts for a statistically significant subsample of the same objects, the empirical methods offer greater accuracy, as well as being far more efficient. These methods use the subsample of the photometric survey with spectroscopically-measured redshifts as a *training set* to constrain the fit of a polynomial function mapping the photometric data as redshift estimators.

Several template based methods have been developed to derive photometric redshifts with increasingly high precision such as *BPZ*<sup>4</sup>, *HyperZ*<sup>5</sup>, *Kcorrect*<sup>6</sup>, *Le PHARE*<sup>7</sup>, *ZEBRA*<sup>8</sup>, *LRT Libraries*<sup>9</sup>, *EAzY*<sup>10</sup>, *Z-PEG*<sup>11</sup>. *Moreover there are also training set based methods, such as AnnZ*<sup>12</sup>, *RFPhotoZ*<sup>13</sup> among others). The variety of methods and approaches and their application to different types of datasets, as well as the adoption of different and often not comparable statistical indicators, make it difficult to evaluate and compare performances in an unambiguous and homogeneous way. Useful but limited in scope blind tests of photo-z's have been performed in Hogg et al. (1998) on spectroscopic data from the Keck telescope on the Hubble Deep Field (HDF), in Hildebrandt et al. (2008) on spectroscopic data from the VIMOS VLT Deep Survey (VVDS; Le Fèvre et al. 2004) and the FORS Deep Field (FDF; Noll et al. 2004, and in Abdalla et al. 2008) on the sample of Luminous Red Galaxies from the SDSS-DR6.

A significant advance in comparing different methods was introduced by Hildebrandt and collaborators (Hildebrandt et al. 2010), with the so called PHAT (PHoto-z Accuracy Testing) contest, which adopts a black-box approach which is typical of benchmarking. Instead of insisting on the subtleties of the data structure, they performed a homogeneous comparison of the performances concentrating the analysis on the last link in the chain: the photo-z's methods themselves.

As pointed out by the authors, in fact, *"it is clear that the two regimes - data and method - cannot be separated cleanly because there are connections between the two. For example, it is highly likely that one method of photo-z estimation will perform better than a second method on one particular dataset while the situation may well be reversed on a different data set."* (cf. Hildebrandt et al. 2010).

Considering that empirical methods are trained on real data and do not require assumptions on the physics of the formation and evolution of stellar populations, Neural Networks (hereafter NNs) are excellent tools to interpolate data and to extract patterns and trends (cf. the standard textbook by Bishop 2006). In this paper we show the application in the PHAT1 contest of the Multi Layer Perceptron (MLP) implemented with a Quasi Newton Algorithm (QNA) as learning rule which has been employed for the first time to interpolate the photometric redshifts.

The present work follows the same path, by having as its aim the testing and probing of the accuracy of the Quasi Newton based Neural Model (MLPQNA) for the derivation of photomet-

ric redshifts. The application of MLPQNA to the photometric redshift estimation of QSO will be presented in Brescia et al. (in preparation).

In Sect. 2 we shortly describe the PHAT contest and the PHAT1 data made available to the contestants and used for the present work. In Sect. 3 we describe the MLPQNA method which was implemented by us and used for the contest, while in Sect. 4 we describe the experiments performed and, in Sect. 5 we present the results derived for us by the PHAT board. Summary and conclusions are wrapped up in Sect. 6.

## 2. The PHAT dataset

First results from the PHAT contest were presented in Hildebrandt et al. (2010), but the contest still continues at the project's web site. PHAT provides a standardized test environment which consists of simulated and observed photometric catalogues complemented with additional materials like filter curves convolved with transmission curves, SED templates, and training sets. The PHAT project has been conceived as a blind contest, still open to host new participants who want to test their own regression method performances, as it was in our case, since we developed our model in the last two years. However, the subsets used to evaluate the performances are still kept secret in order to provide a more reliable comparison of the various methods. Two different datasets are available (see Hildebrandt et al. 2010 for more details).

The first one, indicated as PHAT0, is based on a very limited template set and a long wavelength baseline (from UV to mid-IR). It is composed by a noise-free catalogue with accurate synthetic colors and a catalogue with a low level of additional noise. PHAT0 represents an easy case to test the most basic elements of photo-z estimation and to identify possible low-level discrepancies between the methods.

The second one, which is the one used in the present work, is the PHAT1 dataset, which is based on real data originating from the Great Observatories Origins Deep Survey Northern field (GOODS-North; Giavalisco et al. 2004). According to Hildebrandt et al. (2010), it represents a much more complex environment to test methods to estimate photo-z's, pushing codes to their limits and revealing more systematic difficulties. Both PHAT test datasets are made publicly available through the PHAT website<sup>14</sup> while in Hildebrandt et al. (2010) there is a detailed description of the statistical indicators which were used for the comparison of the results provided by the 21 participants who have so far participated by submitting results obtained with 17 different photo-z codes.

The PHAT1 dataset consists of photometric observations, both from ground and space instruments, presented in Giavalisco et al. (2004), complemented with additional data in other bands derived from Capak et al. (2004). The final dataset covers the full UV-IR range and includes 18 bands: U (from KPNO), B, V, R, I, Z (from SUBARU), F435W, F606W, F775W, F850LP (from HST-ACS), J, H (from ULBCAM), HK (from QUIRC), K (from WIRC) and 3.6, 4.5, 5.8 and 8.0  $\mu$  (from IRAC Spitzer).

The photometric dataset was then cross correlated with spectroscopic data from Cowie et al. (2004); Wirth et al. (2004); Treu et al. (2005), and Reddy et al. (2006). Therefore, the final PHAT1 dataset consists of 1984 objects with 18-band photometry and accurate spectroscopic redshifts. In the publicly available dataset

<sup>4</sup> <http://acs.pha.jhu.edu/txitxo/bpdoc.html>

<sup>5</sup> <http://webast.ast.obs-mip.fr/hyperz/>

<sup>6</sup> <http://cosmo.nyu.edu/blanton/kcorrect/>

<sup>7</sup> <http://www.cfht.hawaii.edu/~arnouts/LEPHARE/lephare.html>

<sup>8</sup> <http://www.exp-astro.phys.ethz.ch/ZEBRA>

<sup>9</sup> <http://www.astronomy.ohio-state.edu/~rjassef/lrt/>

<sup>10</sup> <http://www.astro.yale.edu/eazy/>

<sup>11</sup> <http://imacdlb.iap.fr:8080/cgi-bin/zpeg/zpeg.pl>

<sup>12</sup> <http://www.homepages.ucl.ac.uk/~ucapola/annz.html>

<sup>13</sup> <http://www.sdss.jhu.edu/~carliles/photoZ/RFPhotoZ/>

<sup>14</sup> [http://www.astro.caltech.edu/twiki\\_phat/bin/view/Main/GoodsNorth](http://www.astro.caltech.edu/twiki_phat/bin/view/Main/GoodsNorth)

a little more than one quarter of the objects comes with spectroscopic redshifts and can be used as Knowledge Base (KB) for training empirical methods.

In this contest, in fact, only 515 objects were made available with the corresponding spectroscopic redshift, while for the remaining 1469 objects the related spectroscopic redshift has been hidden to all participants. The immediate consequence is that any empirical method exploited in the contest was constrained to use the 515 objects as training set (knowledge base) and the 1469 objects as the test set, to be delivered to PHAT contest board in order to obtain back the statistical evaluation results. While it is clear that the limited amount of objects in the knowledge base is not sufficient to ensure the best performances of most empirical methods, the fact that all methods must cope with similar difficulties makes the comparison consistent.

### 3. The MLPQNA regression model

MLPQNA stands for the traditional neural network model named Multi Layer Perceptron (MLP; cf. Bishop 2006) implemented with a Quasi Newton Algorithm (QNA) as learning rule. This particular implementation of the traditional MLP's has already been described in Brescia et al. (2012a), and we refer to that paper for a more detailed description in the classification problem context. MLPQNA is made available to the community through the DAMEWARE (DAta Mining & Exploration Web Application REsource; Brescia et al. 2009, 2011, 2012a,b). In the text we also provide the details and the parameters settings for the best performing MLPQNA model so that anyone can easily reproduce the results using the Web Application. User's manuals are available on the DAMEWARE web site<sup>15</sup>. A complete mathematical description of the MLPQNA model is available on the DAME web site<sup>16</sup>. Feed-forward neural networks provide a general framework for representing nonlinear functional mappings between a set of input variables and a set of output variables (Bishop, 2006). One can achieve this goal by representing the nonlinear function of many variables by a composition of non-linear activation functions of one variable, which formally describes the mathematical representation of a feed-forward neural network with two computational layers (Eq. 1):

$$y_k = \sum_{j=0}^M w_{kj}^{(2)} g \left( \sum_{i=0}^d w_{ji}^{(1)} x_i \right) \quad (1)$$

A Multi-Layer Perceptron may be also represented by a graph, as also shown in Fig 1: the input layer ( $x_i$ ) is made of a number of perceptrons equal to the number of input variables ( $d$ ); the output layer, on the other hand, will have as many neurons as the output variables ( $K$ ). The network may have an arbitrary number of hidden layers (in most cases one) which in turn may have an arbitrary number of perceptrons ( $M$ ). In a fully connected feed-forward network each node of a layer is connected to all the nodes in the adjacent layers.

Each connection is represented by an adaptive weight which represents the strength of the synaptic connection between neurons ( $w_{kj}^{(l)}$ ). The response of each perceptron to the inputs is represented by a non-linear function  $g$ , referred to as the activation function. Notice that the above equation assumes a linear activation function for neurons in the output layer. We shall refer to the

topology of an MLP and to the weights matrix of its connections as to the model. In order to find the model that best fits the data, one has to provide the network with a set of examples: the training phase thus requires the KB, i.e. the training set. The learning rule of our MLP is the Quasi Newton Algorithm (QNA) which differs from the Newton Algorithm in terms of the calculation of the hessian of the error function. In fact Newtonian models are variable metric methods used to find local maxima and minima of functions (Davidon, 1968) and, in the case of MLPs they can be used to find the stationary (i.e. the zero gradient) point of the learning function and are the general basis for a whole family of so called Quasi Newton methods.

The traditional Newton method uses the Hessian of a function to find the stationary point of a quadratic form. The Hessian of a function is not always available and in many cases it is far too complex to be computed. More often we can only calculate the function gradient which can be used to derive the Hessian via  $N$  consequent gradient calculations.

The gradient in every point  $\mathbf{w}$  is in fact given by:

$$\nabla E = \mathbf{H} \times (\mathbf{w} - \mathbf{w}^*) \quad (2)$$

where  $\mathbf{w}$  corresponds to the minimum of the error function, which satisfies the condition:

$$\mathbf{w}^* = \mathbf{w} - \mathbf{H}^{-1} \times \nabla E \quad (3)$$

The vector  $-\mathbf{H}^{-1} \times \nabla E$  is known as Newton direction and it is the traditional base for a variety of optimization strategies,

Thus the step of this traditional method is defined as the product of an inverse Hessian matrix and a function gradient. If the function is a positive definite quadratic form, the minimum can be reached in just one step, while in case of an indefinite quadratic form (which has no minimum), we will reach either the maximum or a saddle point. To solve this problem, Quasi Newton methods proceed with a positive definite Hessian approximation. So far, if the Hessian is positive definite, we make the step using the Newton method. If, instead it is indefinite, we first modify it to make it positive definite, and then perform a step using the Newton method, which is always calculated in the direction of the function decrement.

In practice, QNA is an optimization of learning rule based on a statistical approximation of the Hessian by cyclic gradient calculation which, as already mentioned, is at the base of the classical Back Propagation (BP; Bishop 2006) method.

The QNA instead of calculating the  $\mathbf{H}$  matrix and then its inverse, uses a series of intermediate steps of lower computational cost to generate a sequence of matrices which are more and more accurate approximations of  $\mathbf{H}^{-1}$ . During the exploration of the parameter space, in order to find the minimum error direction, QNA starts in the wrong direction. This direction is chosen because at the first step the method has to follow the error gradient and so it takes the direction of steepest descent. However, in subsequent steps, it incorporates information from the gradient. By using the second derivatives, QNA is able to avoid local minima and to follow more precisely the error function trend, revealing a "natural" capability to find the absolute minimum error of the optimization problem.

However, this last feature could be a downside of the model, especially when the signal-to-noise ratio of data is very poor. But with "clean" data, such as in presence of high quality spectroscopic redshifts, used for model training, the QNA performances result extremely precise.

The experiment described in section 4 consists of a supervised regression based on the MLP neural network trained by the

<sup>15</sup> [http://dame.dsf.unina.it/beta\\_info.html](http://dame.dsf.unina.it/beta_info.html)

<sup>16</sup> [http://dame.dsf.unina.it/machine\\_learning.html#mlpqna](http://dame.dsf.unina.it/machine_learning.html#mlpqna)

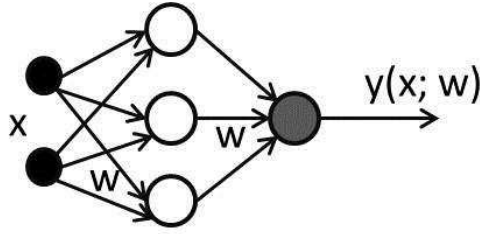


**Fig. 1.** The classical feed-forward architecture of a Multi Layer Perceptron represented as a graph. There are three layers, respectively, input with black nodes, hidden with white nodes and the output represented by a single gray node. At each layer, its nodes are fully connected with each node of the next layer. Each connection is identified by a numerical value called *weight*, usually a real number normalized in the range  $[-1, +1]$ .

Quasi Newton learning rule. As already described, the MLP is a network model composed by input and two computational layers of neurons (see Eq. 1), which propagate submitted data from input to output layer. Each neuron of hidden layer is represented by a non-linear activation function (in our case hyperbolic tangent) of the sum of inputs from all previous layer neurons, multiplied by weights (normalized values in  $[-1, +1]$  representing the connections between neurons, see fig. 1). After propagating the input data, at the final (output) layer, the learning error is evaluated (in our case by means of the Mean Square Error, MSE, between calculated vs desired outputs), and then the backward phase is started, in which a learning rule is applied, by adapting the neuron connection weights in such a way that the error function is minimized. Then the input data are submitted again and a new cycle of learning is achieved. The algorithm stops after a chosen number of iterations or if the error becomes less than a chosen threshold. Note that the error is calculated at each iteration by comparing the calculated value (on all input data) against the desired (*a priori* known) target value. This is the typical approach called “supervised”. When the learning phase is stopped, the trained network is used like a simple function. Input data not used for training, or a mix in case of learning validation, can be submitted to the network, that, if trained well, is able to provide correct output (generalization capability). By looking at the local squared approximation of the error function, it is possible to obtain an expression of minimum position. It is in fact known that the gradient in every point  $w$  of the error surface is given by Eq. 2. The network is trained in order to learn to calculate the correct photometric redshift given the input features for each object (see section 4). This is indeed a typical supervised regression problem.

In terms of computational cost, the implementation of QNA can be problematic. In fact to approximate the inverse Hessian matrix it requires to generate and to store  $N \times N$  approximations, where  $N$  is the number of variables and so the number of gradients involved in the calculation. So far, given  $nI$  the number of iterations chosen by the user, the total computational cost is about  $nI * N^2$  floating point per second (flops). For this reason it exists a family of quasi-newton optimization methods, which allow to improve the complexity of the algorithm. In particular, in our implementation, we use the limited-memory BFGS (L-BFGS; Byrd et al. 1994; Broyden 1970; Fletcher 1970; Goldfarb 1970; Shanno 1970), where BFGS is the acronym composed by the names of the four inventors.

L-BFGS never stores the full  $N$  approximations of the hessian matrix, but only the last  $M$  steps (with  $M \ll N$ ). Hence, given  $M$  the stored approximation steps, the computational cost could be reduced to about  $nI * (N * M)$  flops, which in practice transforms the total cost of the algorithm from an exponential form to a polynomial one. Moreover, in order to give a complete computational complexity evaluation for the implementation of the

MLPQNA model, it remains to analyze the feed-forward part of the algorithm, for instance the computational flow of input patterns throughout the MLP network, up to the calculation of the network error (as said the MSE between the desired spectroscopic redshift and the one calculated by the network), at each training iteration after a complete submission of all input patterns.

The feed-forward phase involves the flow of each input pattern throughout the network, from the input to output layer, passing through the hidden layer. This phase can be described by the following processing steps (Mizutani & Dreyfus 2001):

- *Process 1 (P1)*: network node input computation;
- *Process 2 (P2)*: network node activation function computation;
- *Process 3 (P3)*: error evaluation;

The computational cost, in terms of needed flops, for the above three processing steps, can be summarized as follows.

Given  $d$  the number of training data,  $N_w$  the number of network weights,  $A_f$  and  $N_n$  respectively, the flops needed to execute the activation function (strongly depending on the hosting computer capabilities) and number of nodes present in the hidden plus output layers,  $O_n$  the number of output nodes, we obtain:

$$P1 \cong d \times N_w \quad (4)$$

$$P2 \cong d \times A_f \times N_n \quad (5)$$

$$P3 \cong d \times O_n \quad (6)$$

In conclusion, the computational cost for the feed-forward phase of the MLPQNA algorithm has a polynomial form of about  $nI * d \times [N_w + (A_f \times N_n) + O_n]$ . The total complexity of MLPQNA implementation is hence obtained by the polynomial expansion of Eq. 7, as the sum of feed-forward and backward phases multiplied by the number of training iterations.

$$flops \cong nI * [(d \times (N_w + (A_f \times N_n) + O_n)) + (N * M)] \quad (7)$$

Considering our training experiment described in Sect. 4.3 and using parameters reported in Tab. 2, from Eq. 7 we obtain about 1200 Gflops, which corresponds to about 15 min of execution time.

#### 4. The experiment Workflow

In this section we describe the details of the sequence of concatenated computational steps performed in order to determine photometric redshifts. This is what we intended as a workflow, which can be seen also as the description of the procedure building blocks.

MLPQNA method was applied by following the standard

Machine Learning (ML) workflow (Bishop 2006), which is here summarized: *i*) extraction of the KB by using the 515 available spectroscopic redshifts; *ii*) determination of the "optimal" model parameter setup, including pruning of data features and training/test with the available KB; *iii*) application of the tuned model to measure photometric redshifts on the whole PHAT1 dataset of  $N=1984$  objects, by including also the re-training on the extended KB. We also follow the rules of the PHAT1 contest, applying the new method in two different ways, first to the whole set of 18 bands and then to the 14 non-IRAC bands only. In order to better clarify what is deeply discussed in the next sub-sections, it is important to stress that the 515 objects, with spectroscopic redshifts publicly available, have been used to tune our model. In practice, 400 objects have been used as training set and the remaining 115 as test/validation set (steps *i*) and *ii*) of the workflow, see Sect.s 4.1, 4.2). After having tuned our model, we performed a full training on all 515 objects, in order to exploit all the available knowledge base (see Sect. 4.3).

#### 4.1. Extraction of the Knowledge Base

For supervised methods it is common praxis to split the KB in at least three disjoint subsets: one (training set) to be used for training purposes, i.e. to teach the method how to perform the regression; the second one (validation set) to check against loss of generalization capabilities (also known as overfitting); and the third one (test set) to be used to evaluate the performances of the model. As a rule of thumb, these sets should be populated with 60%, 20% and 20% of the objects in the KB, respectively. In order to ensure a proper coverage of the Parameter Space (PS), objects in the KB are split among the three datasets by random extraction and usually this process is iterated several times in order to minimize biases introduced by fluctuations in the coverage of the PS.

In the case of MLPQNA described here, we used cross-validation (cf. Geisser 1975) in order to minimize the size of the validation set ( $\sim 10\%$ ). Training and validation were therefore performed together using as training set  $\sim 80\%$  of the objects and as test set the remaining  $\sim 20\%$  (in practice 400 records in the training set and 115 in the test set). In order to ensure a proper coverage of the PS we checked that the randomly extracted populations had a spec- $z$  distribution compatible with that of the whole KB. The automatized process of the cross-validation was done by performing 10 different training runs with the following procedure: (i) we split the training set into 10 random subsets, each one composed by 10% of the dataset; (ii) at each training run we apply the 90% of the dataset for training and the excluded 10% for validation. This procedure is able to avoid overfitting on the training set (Bishop 2006). There are several variants of cross validation methods (Sylvain & Celisse, 2010). We in particular have chosen the  $k$ -fold cross validation, particularly suited in presence of a scarcity of known data samples (Geisser, 1975). Since the Eq. 7 is referred to a single training run, in case of application of the  $k$ -fold cross validation procedure, the execution time could be estimated by multiplying the Eq. 7 by the factor  $k - 1$ , where  $k$  is the total number of runs.

#### 4.2. Model optimization

As known, supervised machine learning models are powerful methods able to learn from training data the hidden correlation between input and output features. Of course, their generalization and prediction capabilities strongly depend by the intrinsic

quality of data (signal-to-noise ratio), level of correlation inside of the PS and by the amount of missing data present in the dataset. Among the factors which affect performances, the most relevant is the fact that most ML methods are strongly sensitive to the presence of Not a Number (NaN) in the dataset to be analysed (Vashist & Garg 2012). This is especially relevant in astronomical dataset where NaN's may either be non detections (i.e. objects which in a given band are observed but non detected since they are below the detection threshold) or related to patches of the sky which have not been observed. The presence of features with a large fraction of NaN's can seriously affect the performances of a given model and lower the accuracy or the generalization capabilities of a specific model. It is therefore a good praxis to analyze the performances of a specific model in presence of features with large fractions of NaN's. This procedure is strictly related to the so called feature selection or "pruning of the features" phase which consists in evaluating the significance of individual features to the solution of a specific problem. In what follows we shall shortly discuss the outcome of the "pruning" performed on the PHAT1 dataset.

##### 4.2.1. Pruning of features

It is also necessary to underline that especially in presence of small datasets there is a need for a compromise: while on the one hand it is necessary to minimize the effects of NaN's, on the other it is not possible to simply remove each record containing a NaN, because otherwise too much information would be lost.

In table 1 we list the percentage of NaN's in each photometric band both in the training and full datasets. Poor features, namely the fluxes in the K and m5.8 bands were not used for the subsequent analysis.

The pruning was performed separately on the two PHAT1 datasets (18-bands and 14-bands), respectively. A total of 37 experiments was run on the two datasets: the various experiments differing in the groups of features removed. We started by considering all features (bands), removing the two worst bands, for instance K and m5.8, which outlier quantity was over the 15% of patterns. Then a series of experiments was performed by removing one band at a time, by considering the NaN's percentage shown in table 1.

##### 4.2.2. Performance metrics

The performances of the various experiments were evaluated (as done in the PHAT contest) in terms of:

- *scatter*: is the RMS of  $\Delta z$
- *bias*: is the mean of  $\Delta z$
- *fraction of outliers*: where outliers are defined by the condition:  $|\Delta z| > 0.15$

Where:

$$\Delta z \equiv \frac{z_{spec} - z_{phot}}{1 + z_{spec}} \quad (8)$$

At the end of this process, we obtained the best results, reported in table 2.

#### 4.3. Application to the PHAT1 dataset

We performed a series of experiments in order to fine tune the model parameters, whose best values are:

MLP network topology parameters (see Tab. 2):

BAND	Dataset Column ID	% NaN in whole set	% NaN in Training	NaN % Absolute Difference
m5.8	17	19.35	17.28	2.07
K	14	17.14	18.64	1.5
HK	13	5.65	6.21	0.57
m8	18	3.48	3.5	0.02
F435W	7	2.67	1.75	0.92
H	12	2.37	2.52	0.16
J	11	1.16	1.55	0.39
U	1	1.01	1.17	0.16
R	4	0.15	0.19	0.04
B	2	0.1	0.19	0.09
V	3	0.05	0.19	0.14
F606W	8	0.05	0	0.05
m 3.6	15	0.05	0	0.05
I	5	0	0	0
Z	6	0	0	0
F775W	9	0	0	0
F850LP	10	0	0	0
m4.5	16	0	0	0

**Table 1.** The percentages of Not a Number in the whole dataset (col 3), with 1984 objects and in the trainset (col 4), with 515 objects, for each band. The last column reports the absolute differences between the two NaN percentages. As shown this difference remains always under 3%, demonstrating that the two datasets are congruent in terms of NaN quantity.

exp. n	missing features	feat.	hid.	step	res.	dec.	MxIt	CV	scatter	outliers%	bias
37	m5.8,K, HK, m8	14	29	0.0001	30	0.1	3000	10	0.057	22.61%	-0.0077
26	m5.8, K, m3.6, m4.5, HK, m8	12	25	0.0001	30	0.1	3000	10	0.062	17.39%	0.0078

**Table 2.** Description of the best experiments for the 18 bands (Exp. n. 37) and the 14 bands datasets (Exp. n. 26). Column 1: sequential experiment identification code; column 2: features not used in the experiment; columns 3-4: number of input (features) and hidden neurons; column 5-9: parameters of the MLPQNA used during the experiment; column 10: scatter error evaluated as described in the text; column 11: fraction of outliers; column 12: bias.

- feat: 14 (12) input neurons (corresponding to the pruned number of input band magnitudes listed in Tab. 1);
- hid: 29 (25) hidden neurons;
- 1 output neuron.

QNA training rule parameters (see Tab. 2):

- step: 0.0001 (one of the two stopping criteria. The algorithm stops if approximation error step size is less than this value. A step value equal to zero means to use the parameter MxIt as unique stopping criterion.);
- res : 30 (number of restarts of hessian approximation from random positions, performed at each iteration);
- dec : 0.1 (regularization factor for weight decay. The term  $dec * ||networkweights||^2$  is added to the error function, where  $networkweights$  is the total number of weights in the network. When properly chosen, the generalization error of the network is highly improved);
- MxIt: 3000 (max number of iterations of hessian approximation. If zero the step parameter is used as stopping criterion);
- CV: 10 (k-fold Cross Validation, with k=10. This parameter is described in section 4.1).

With such parameters, we obtained the statistical results (in terms of scatter, bias and outlier percentage) as reported in the last three columns of Tab. 2.

Once the model optimization described above had been determined, the MLPQNA was re-trained on the whole KB (515 objects) and applied to the whole PHAT1 dataset (1984 objects), which was then submitted to the PHAT contest for final evaluation (see below).

Details of the experiments can be found at the DAME web site<sup>17</sup>, while the parameter settings and the results for the best models are summarised in table 3.

## 5. The PHAT1 results and comparison with other models

With the model trained as described in the above section, we calculated photometric redshifts for the entire PHAT1 dataset, i.e. also for the remaining 1469 objects, for which the corresponding spectroscopic redshift was hidden to the contest participants, obtaining a final photometric catalogue of 1984 objects. This output catalogue has been finally delivered to PHAT contest board, receiving as feedback the statistical results (scatter, bias and outlier's percentage) coming from the comparison between spectroscopic and photometric information, in both cases (18 and 14 bands).

So far, the statistical results and plots referred to the whole data sample, which is kept secret to all participants as required by the PHAT contest, were provided by H. Hildebrandt and reported also in the PHAT Contest wiki site<sup>18</sup>. So far, the results obtained by analysing the photometric redshifts calculated by MLPQNA, are shown in table 3.

The most significant results can be summarized as it follows:

<sup>17</sup> [http://dame.dsf.unina.it/dame\\_photoz.html](http://dame.dsf.unina.it/dame_photoz.html)

<sup>18</sup> [http://www.astro.caltech.edu/twiki\\_phat/bin/view/Main/GoodsNorthResults#Cavuoti\\_Stefano\\_et\\_al\\_neural\\_net](http://www.astro.caltech.edu/twiki_phat/bin/view/Main/GoodsNorthResults#Cavuoti_Stefano_et_al_neural_net)

- i) 18-band experiment: 324 outliers with  $|\Delta_z| > 0.15$ , corresponding to a relative fraction of 16.33%. For the remaining 1660 objects bias and rms are:  $0.000604251 \pm 0.0562278$
- ii) 14-band experiment: 384 outliers with  $|\Delta_z| > 0.15$ , corresponding to a relative fraction of 19.35%. 1600 objects with bias and variance  $0.00277721 \pm 0.0626341$ .

A more detailed characterization of the results can be found in the first line of parts A, B and C in the table 3, while figure 2, provided by H. Hildebrandt, gives the scatter plots (spec-z's vs photo-z's) for the 18 and 14 bands, respectively.

In order to compare our results with other models, we also report in table 3 the statistical indicators for the other empirical methods which competed in the PHAT1 contest. The methods are:

- **AN-e**: ANNz, Artificial Neural Network, an empirical photo-z code based on artificial neural networks (Collister & Lahav, 2004);
- **EC-e**: Empirical  $\chi^2$ , a subclass of kernel regression methods; which mimics a template-based technique with the main difference that an empirical dataset is used in place of the template grid (Wolf, 2009);
- **PO-e**: Polynomial Fit, a "nearest neighbour" empirical photo-z method based on a polynomial fit so that the galaxy redshift is expressed as the sum of its magnitudes and colours (Li & Yee, 2008);
- **RT-e**: Regression Trees, based on Random Forests which are an empirical, non-parametric regression technique (Carliles et al., 2010).

More details can be found in the quoted references and in Hildebrandt et al. (2010).

For each of the datasets (18 and 14 bands), statistics in Table 3 refers to several regimes: the first one (A) defines as outliers all objects having  $|\Delta_z| > 0.15$  and it is divided into two subsections: the left side includes all objects, while the right side includes objects brighter than  $R = 24$ ; the second one (B) defines as outliers objects having  $|\Delta_z| > 0.50$  and it is divided as section (A); the third one (C) defines as outliers objects having  $|\Delta_z| > 0.50$  and divided into a left side, for object with  $z \leq 1.5$  and a right side having  $z > 1.5$ .

By analyzing the MLPQNA performance in the different regimes, we obtained:

*All objects*: in the 18 bands experiment, QNA scores the best results in term of bias, and gives comparable results with PO-e in terms of scatter and number of outliers. In fact, while in Part A the scatter is slightly larger than those of PO-e method (0.052 against 0.056), the number of outliers is lower (18.0% against 16.3%) and in Part. B is the viceversa (0.124 against 0.114 and 3.1% against 3.8%). In the 14 band experiment QNA obtains values slightly higher than PO-e in terms of scatter (0.051 against 0.063) and than EC-e in terms of bias (0.002 against 0.0028). For what concerns the fraction of outliers QNA scores results larger than PO-e and EC-e (13.7% and 16.7% against 19.3%).

*Bright objects*: for bright objects ( $R < 24$ ), the QNA resulting bias is again the best within the different empirical methods, while for scatter and number of outliers, QNA obtains values slightly higher than PO-e in both the 18 (0.047 against 0.053 and 10.7% against 11.7%) and the 14 bands datasets (0.046 against 0.060 and 7.1% against 13.7%).

*Distant vs near objects*: in the distant sample ( $z_{sp} > 1.5$ ) QNA scores as first in terms of bias, scatter, and number of outliers for 18 bands. In the 14 band dataset case, it results the best

method in terms of scatter, but with a bias (0.015 against 0.0222) and number of outliers (29.5% against 35.0%) higher than EC-e. In the near sample ( $z_{sp} < 1.5$ ) QNA is the best in terms of bias. The scatter is slightly higher than PO-e's for both 18 (0.049 against 0.053) and 14 bands (0.047 against 0.061). For what concerns outliers, PO-e performs better at 18 bands (12.6% against 14.6%), while PO-e and EC-e perform better at 14 bands (9.4% and 14.5% against 16.6%).

## 6. Summary and Conclusions

For the first time the MultiLayer Perceptron with Quasi Newton learning rule described here has been exploited to solve regression problems in the astrophysical context. This method was applied on the whole PHAT1 dataset of  $N=1984$  objects (Hildebrandt et al. (2010)) to determine photometric redshifts after an optimization of the model performed by using as a training set the 515 available spectroscopic redshifts.

The statistics obtained by the PHAT board, by analyzing the photometric redshifts derived with MLPQNA, and the comparison with other empirical models are reported in Table 3.

From a quick inspection of table 3, it descends that it does not exist an empirical method which can be regarded as the best in terms of all the indicators (e.g. bias, scatter and number of outliers) and that EC-e (Empirical  $\chi^2$  method), PO-e (Polynomial Fit method) and MLPQNA produce comparable results. However, the MLPQNA method, on average, gives the best result in terms of bias at any regime.

For what the scatter is concerned, by considering the dataset with 18 bands reported in Parts A and B of table 3, MLPQNA obtains results comparable with the PO-e method. In fact, in Part A PO-e's scatter is better than MLPQNA's, but with a larger number of outliers; while the trend is reversed in Part B. In the other cases both the scatter and number of outliers are slightly worse than PO-e and EC-e methods.

In general, MLPQNA seems to have better generalization capabilities than most other empirical methods especially in presence of underpopulated regions of the Knowledge Base. In fact,  $\sim 500$  objects with spectroscopic redshifts spread over such a large redshift interval are by far not sufficient to train most other empirical codes on the data. This was also pointed out also by Hildebrandt et al. (2010), who noticed that the high fraction of outliers produced by empirical methods is on average higher than what is currently found in literature ( $\sim 7.5\%$ ) and explained it as an effect of the small size of the training sample, which maps poorly the very large range in redshifts and does not include a large enough number of objects with peculiar SED's.

In this respect we wish to stress that as it has already been shown in another application (cf. Brescia et al. 2012a) and will be more extensively discussed in a forthcoming paper, MLPQNA enjoys the very rare prerogative of being able to obtain good performances also when the KB is small and thus under-sampled (Brescia et al. in preparation).

### Acknowledgements.

The authors wish to thank the anonymous referee for useful comments which improved the paper. The authors wish also to thank H. Hildebrandt for the courtesy to provide statistical results and plots, all present and former members of the DAME collaboration and in particular R. D'Abrusco for useful discussions. DAME has been funded through several grants which are mentioned on the collaboration web site. We acknowledge the use of TOPCAT and of other Virtual Observatory tools during some steps of the procedure. GL wishes to thank the California Institute of Technology for the kind hospitality. AM

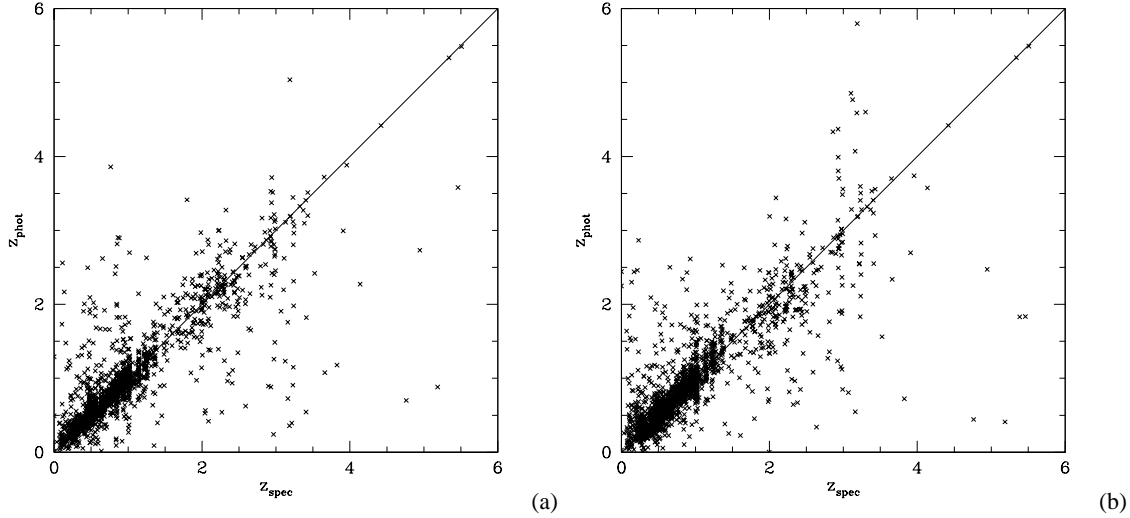


**Fig. 2.** Results obtained by our model and provided by the PHAT contest board in terms of direct comparison between our photometric and blind spectroscopic information. In the (a) panel are plotted the photometric vs. spectroscopic redshifts for the whole dataset using 10 photometric bands (Experiment 37). In panel (b) the same but using only 14 photometric bands (Experiment 26). (Courtesy of H. Hildebrandt).

<b>A</b>	18-band; $ \Delta z  \leq 0.15$			14-band; $ \Delta z  \leq 0.15$			18-band; $R < 24$ ; $ \Delta z  \leq 0.15$			14-band; $R < 24$ ; $ \Delta z  \leq 0.15$		
Code	bias	scatter	outliers %	bias	scatter	outliers %	bias	scatter	outliers %	bias	scatter	outliers %
QNA	0.0006	0.056	16.3	0.0028	0.063	19.3	0.0002	0.053	11.7	0.0016	0.060	13.7
AN-e	-0.010	0.074	31.0	-0.006	0.078	38.5	-0.013	0.071	24.4	-0.007	0.076	32.8
EC-e	-0.001	0.067	18.4	0.002	0.066	16.7	-0.006	0.064	14.5	-0.003	0.064	13.5
PO-e	-0.009	0.052	18.0	-0.007	0.051	13.7	-0.009	0.047	10.7	-0.008	0.046	7.1
RT-e	-0.009	0.066	21.4	-0.008	0.067	24.2	-0.012	0.063	16.4	-0.012	0.064	18.4
<b>B</b>	18-band; $ \Delta z  \leq 0.5$			14-band; $ \Delta z  \leq 0.5$			18-band; $R < 24$ ; $ \Delta z  \leq 0.5$			14-band; $R < 24$ ; $ \Delta z  \leq 0.5$		
Code	bias	scatter	outliers %	bias	scatter	outliers %	bias	scatter	outliers %	bias	scatter	outliers %
QNA	-0.0028	0.114	3.8	-0.0046	0.125	3.8	-0.0039	0.101	1.7	-0.0039	0.101	1.7
AN-e	-0.036	0.151	3.1	-0.035	0.173	4.2	-0.047	0.130	1.4	-0.047	0.130	1.4
EC-e	-0.007	0.120	3.6	-0.003	0.114	3.6	-0.015	0.106	1.9	-0.015	0.106	1.9
PO-e	-0.013	0.124	3.1	0.001	0.107	2.3	-0.020	0.098	1.2	-0.020	0.098	1.2
RT-e	-0.031	0.126	3.2	-0.028	0.137	3.6	-0.034	0.111	1.4	-0.034	0.111	1.4
<b>C</b>	18-band; $z_{sp} \leq 1.5$ , $ \Delta z  \leq 0.15$			14-band; $z_{sp} \leq 1.5$ , $ \Delta z  \leq 0.15$			18-band; $z_{sp} > 1.5$ , $ \Delta z  \leq 0.15$			14-band; $z_{sp} > 1.5$ , $ \Delta z  \leq 0.15$		
Code	bias	scatter	outliers %	bias	scatter	outliers %	bias	scatter	outliers %	bias	scatter	outliers %
QNA	-0.0004	0.053	14.6	0.0001	0.061	16.6	0.0074	0.072	26.3	0.0222	0.070	35.0
AN-e	-0.017	0.070	27.6	-0.010	0.076	33.6	0.051	0.078	50.7	0.045	0.077	66.4
EC-e	-0.003	0.065	16.1	-0.000	0.064	14.5	0.015	0.077	32.3	0.015	0.077	29.5
PO-e	-0.012	0.049	12.6	-0.011	0.047	9.4	0.019	0.075	48.3	0.026	0.074	37.7
RT-e	-0.016	0.062	19.6	-0.014	0.064	21.1	0.040	0.072	31.8	0.039	0.071	41.9

**Table 3.** Comparison of the performances of our MLPQNA (here labeled as QNA) method against all other empirical methods analysed by PHAT board. For a description of other methods (namely AN-e, EC-e, PO-e and RT-e) see the text. The table is divided into three parts (namely A, B and C). Data for the other empirical method have been extracted from Hildebrandt et al. (2010). In each part of the table we list the results (on both the 18 and the 14 bands datasets) for a specific subsample of the PHAT objects. Part A: statistical indicators (bias and scatter) for the 18 and 14 bands computed on objects with  $|\Delta z| \leq 0.15$  and for objects with  $|\Delta z| \leq 0.15$  and  $R < 24$ . The column “outliers” gives the fraction of outliers defined as objects with  $|\Delta z| > 0.15$ . Part B: the same but for  $|\Delta z| \leq 0.5$ . Part C: the same but for objects with spectroscopic redshift  $z_{sp} \leq 1.5$  and  $|\Delta z| \leq 0.15$ , and for  $z_{sp} > 1.5$  and  $|\Delta z| \leq 0.15$ . The definitions of bias, scatter and outliers fraction are given in the text. Values were computed by the PHAT collaboration on the whole PHAT1 dataset.

and MB wish to thank the financial support of PRIN-INAF 2010, “Architecture and Tomography of Galaxy Clusters”.

## References

- Abdalla, F. B., Banerji, M., Lahav, O., & Rashkov, V. 2008, [arXiv:astro-ph/0812.3831]
- Albrecht, A., Bernstein, G., Cahn, R. et al., 2006, Report of the Dark Energy Task Force (astro-ph/0609591)
- Bishop, C.M., Pattern Recognition and Machine Learning, 2006, Springer ISBN 0-387-31073-8
- Brescia, M., et al., 2009, Mem. SAI Suppl, 13, 56
- Brescia, M., Cavuoti, S., D’Abrusco, R., Laurino, O. & Longo, G. 2011, V International Workshop on Distributed Cooperative Laboratories: “Instrumenting the Grid”, in Remote Instrumentation for eScience and Related Aspects, 2011, F. Davoli et al. (eds.), Springer:NY
- Brescia, M., Cavuoti, S., Paolillo, M., Longo, G. & Puzia, T. 2012a, MNRAS, 421, issue 2, 1155
- Brescia, M., Longo, G., Castellani, M. et al., 2012b, Mem. SAI Suppl, 19, 324
- Broyden, C. G., 1970, Journ. of the Inst. of Math. and Its Appl., 6, 76
- Byrd, R.H., Nocedal, J., Schnabel, R.B., 1994, Mathematical Programming, 63, 4, pp. 129-156
- Capak, P., Cowie, L. L., Hu, E. M., et al. 2004, AJ, 127, 180
- Capozzi, D., De Filippis, E., Paolillo, M., D’Abrusco, R., Longo G., 2009, MNRAS, 396, 900



- Carliles, S., Budavári, T., Heinis, S., Priebe, C., & Szalay, A. S. 2010, *ApJ*, 712, 511
- Collister, A. A., & Lahav, O. 2004, *PASP*, 116, 345
- Cowie, L. L., Barger, A. J., Hu, E. M., Capak, P., & Songaila, A. 2004, *AJ*, 127, 3137
- Csabai, I., et al. 2003, *AJ*, 125, 580
- D'Abrusco, R., Staiano, A., Longo, G. et al. 2007, *ApJ*, 663, 752
- Davidon, W.C., 1968, *Comput. J.* 10, 406
- Euclid Red Book, ESA Technical Document, 2011, ESA/SRE(2011)12, Issue 1.1, [arXiv:astro-ph/1110.3193]
- Fletcher, R., 1970, *Computer Journal* 13: 317
- Giavalisco, M., Ferguson, H. C., Koekemoer, A. M., et al. 2004, *ApJ*, 600, L93
- Geisser, S., 1975, *Journal of the American Statistical Association*, 70 (350), 320-328
- Goldfarb, D., 1970, *Mathematics of Computation*, 24, 23
- Hildebrandt, H., Wolf, C., & Benitez, N., 2008, *AA*, 480, 703
- Hildebrandt, H., Arnouts, S., Capak, P., Wolf, C. et al. 2010, *AA*, 523, 31
- Hogg D.W., Cohen, J.G., Blandford, R., et al. 1998, *ApJ*, 115, 1418
- Huterer, D.; Takada, M., Bernstein, G., Jain, B., 2006, *MNRAS* 366, 101
- Koo, D.C., 1999, *Astronomical Society of the Pacific Conference Series*, vol. 191, 3, edited by Weymann, Storrie-Lombardi, Sawicki & Brunner.
- Keichi, U., Medezinski, E., Nonino, M., et al. 2012, *ApJ Submitted*, arXiv:1204.3630.
- Le Fèvre, O., Vettolani, G., Paltani, S., et al. 2004, *AA*, 428, 1043
- Li, I. H. & Yee, H. K. C. 2008, *AJ*, 135, 809
- Massarotti, M., Iovino, A., & Buzzoni, A. 2001a, *A&A*, 368, 74
- Massarotti, M., Iovino, A., Buzzoni, A., & Valls-Gabaud, D. 2001b, *A&A*, 380, 425
- Mizutani, E. and Dreyfus, S. E. 2001, On complexity analysis of supervised MLP-learning for algorithmic comparisons. In Proceedings of the 14th INNS-IEEE International Joint Conference on Neural Networks (IJCNN) (Washington, DC, Jul.) 347, 352
- Noll, S., Mehlert, D., Appenzeller, I., et al. 2004, *AA*, 418, 885
- Peacock, J. A., Schneider, P., Efstathiou, G., et al. 2006, ESA-ESO Working Group on Fundamental Cosmology, Tech. Rep.
- Reddy, N. A., Steidel, C. C., Erb, D. K., Shapley, A. E., & Pettini, M. 2006, *ApJ*, 653, 1004
- Shanno, D. F., 1970, *Math. Comput.* 24: 647
- Sylvain, A., & Celisse, A., 2010, A survey of cross-validation procedures for model selection. *Statistics Surveys*, 4, 40-79. doi: 10.1214/09-SS054
- Treu, T., Ellis, R. S., Liao, T. X., & van Dokkum, P. G. 2005, *ApJ*, 633, 174
- Vashist, R., & Garg, M. L. 2012, A Rough Set Approach for Generation and Validation of Rules for Missing Attribute Values of a Data Set, *IJCA* (0975-8887), Volume 42, N. 14, 31, 35
- Wirth, G. D., Willmer, C. N. A., Amico, P., et al. 2004, *AJ*, 127, 3121
- Wolf, C., 2009, *MNRAS*, 397, 520